Determination of a Morphological Phase Diagram of Titania/Titanate Nanostructures from Alkaline Hydrothermal Treatment of Degussa P25

Dana L. Morgan,* Huai-Yong Zhu, Ray L. Frost, and Eric R. Waclawik

Inorganic Materials Research Program, School of Physical and Chemical Sciences, Queensland University of Technology, GPO Box 2434, Brisbane QLD 4001, Australia

Received January 9, 2008
Revised Manuscript Received May 9, 2008

The controlled manipulation of low-dimensional forms of metal oxides has generated much interest in the literature, especially nanotubes generated from TiO_2. Various methods of TiO_2 nanotube production have been employed throughout the literature involving anodic oxidation,[1] hydrothermal treatment,[2,3] and templating.[4] Since the innovative work of Kasuga et al.,[2a,b] soft-chemical hydrothermal treatment (alkaline hydrothermal treatment)[3] has gained a strong following with keen interest in potential applications such as photocatalysts,[5] sorbents,[6,7] Li- and H- storage,[3c,8,9] and biomedical applications.[2c,d] Such keen interest and high throughput of research has sparked numerous debates focusing predominantly on the phase and composition of the resultant nanotubes and their mechanism of formation, as recently reviewed by Bavykin et al.[3b] Both nanotubes and nanoribbons are synthesized by the reaction between TiO_2 solids and NaOH under hydrothermal conditions and are layered titanates. Interestingly, subtle changes in the synthesis conditions may lead to marked differences in the structural properties. For instance, the nanotubes have a specific surface area of ~ 300 m^2/g, whereas the surface areas of nanoribbons are in a range between 30 and 50 m^2/g.[10]

Although nanotubes are primarily formed through the alkaline hydrothermal treatment of TiO_2 solids, nanoribbons are observed under harsher hydrothermal conditions (higher NaOH concentrations and temperatures).[3a,11–17] These 1D nanostructures may be grouped generally into four typical morphologies: nanotubes, nanorods, nanowire/nanofibers, and nanobelt/nanoribbons.[18] Although the nanostructures formed under harsher alkaline hydrothermal treatments have been described as nanofibers and nanorods,[3a,11] their structures conform toward nanobelt/nanoribbon classification.[18] Nanowire morphologies, however, have been observed after post treatments or longer treatment durations of the preliminary nanotube synthesis.[12,13] Hydrothermal liquours other than caustic solutions for nanotube production include Na_2S and H_2O: with only Na_2S solutions producing nanotubes of similar dimensions.[19,20]

Following the Kasuga method,[2] there are a number of parameters that affect the nanostructure formation and phase including: caustic concentration; temperature; treatment duration; post-treatments (washing, calcination, chemical treatment); and starting materials (amorphous, crystalline, commercial, self-prepared, anatase, rutile and brookite). A common trend in alkaline hydrothermal treatments is to either maintain set hydrothermal parameters (only altering the post-treatments),[12] or to alter select hydrothermal parameters to determine specific effects of individual parameters.[3a,13,14] To date, comprehensive examination of the relationship between hydrothermal parameters, product morphology and phase has not been studied as exclusively. Through previous studies, parallels have been established between the parametric effects on the nanostructure formation, however, the overall morphological evolution due to caustic concentration and hydrothermal temperature has not previously been established.

This study involved the systematic investigation of caustic concentration and temperature treatment on nanostructure formation from Degussa P25 through alkaline hydrothermal treatment via the Kasuga method,[2] for a set duration of 20 h. The hydrothermal conditions chosen (5−10 mol dm^{-3} NaOH, 100−220 °C) encompass the conditions generally employed throughout the literature (moderate to extreme

* Corresponding author. E-mail: dl.morgan@qut.edu.au.

(1) (a) Gong, D.; Grimes, C. A.; Varghese, O. K.; Hu, W.; Singh, R. S.; Chen, Z.; Dickey, E. C. *J. Mater. Res.* **2001**, *16*, 3331–3334. (b) Wang, W.; Varghese, O. K.; Paulose, M.; Grimes, C. A. *J. Mater. Res.* **2004**, *19*, 417–422.
(2) (a) Kasuga, T.; Hiramatsu, M.; Hoson, A.; Sekino, T.; Niihara, K. *Adv. Mater.* **1999**, *11*, 1307–1311. (b) Kasuga, T.; Hiramatsu, M.; Hoson, A.; Sekino, T.; Niihara, K. *Langmuir* **1998**, *14*, 3160–3163. (c) Kasuga, T. *Thin Solid Films* **2006**, *496*, 141–145. (d) Kubota, S.; Johkura, K.; Asanuma, K.; Okouchi, Y.; Ogiwara, N.; Sasaki, K.; Kasuga, T. *J. Mater. Sci. Mater. Med.* **2004**, *15*, 1031–1035.
(3) (a) Bavykin, D. V.; Parmon, V. N.; Lapkin, A. A.; Walsh, F. C. *J. Mater. Chem.* **2004**, *14*, 3370–3377. (b) Bavykin, D. V.; Friedrich, J. M.; Walsh, F. C. *Adv. Mater.* **2006**, *18*, 2807–2824. (c) Bavykin, D. V.; Lapkin, A. A.; Plucinski, P. K.; Friedrich, J. M.; Walsh, F. C. *J. Phys. Chem. B* **2005**, *109*, 19422–19427.
(4) Jung, J. H.; Kobayashi, H.; van Bommel, K. J. C.; Shinkai, S.; Shimizu, T. *Chem. Mater.* **2002**, *14*, 1445–1447.
(5) Xu, J.-C.; Lu, M.; Guo, X.-Y.; Li, H.-L. *J. Mol. Catal. A: Chem.* **2005**, *226*, 123–127.
(6) Kleinhammes, A.; Wagner, G. W.; Kulkarni, H.; Jia, Y.; Zhang, Q.; Qin, L.-C.; Wu, Y. *Chem. Phys. Lett.* **2005**, *411*, 81–85.
(7) Umek, P.; Cevc, P.; Jesih, A.; Gloter, A.; Ewels, C. P.; Arčon, D. *Chem. Mater.* **2005**, *17*, 5945–5950.
(8) Kavan, L.; Kalbáč, M.; Zukalová, M.; Exnar, I.; Lorenzen, V.; Nesper, R.; Graetzel, M. *Chem. Mater.* **2004**, *16*, 477–485.
(9) Li, J.; Tang, Z.; Zhang, Z. *Electrochem. Commun.* **2005**, *7*, 62–67.
(10) (a) Lan, Y.; Gao, X.; Zhu, H.; Zheng, Z.; Yan, T.; Wu, F.; Ringer, S. P.; Song, D. *Adv. Funct. Mater.* **2005**, *15*, 1310–1318. (b) Zhu, H. Y.; Lan, Y.; Gao, X. P.; Ringer, S. P.; Zheng, Z. F.; Song, D. Y.; Zhao, J. C. *J. Am. Chem. Soc.* **2005**, *127*, 6730–6736.
(11) Kolen'ko, Y. V.; Kovnir, K. A.; Gavrilov, A. I.; Garshev, A. V.; Frantti, J.; Lebedev, O. I.; Churagulov, B. R.; Van Tendeloo, G.; Yoshimura, M. *J. Phys. Chem. B* **2006**, *110*, 4030–4038.
(12) Poudel, B.; Wang, W. Z.; Dames, C.; Huang, J. Y.; Kunwar, S.; Wang, D. Z.; Banerjee, D.; Chen, G.; Ren, Z. F. *Nanotechnology* **2005**, *16*, 1935–1940.
(13) Horváth, E.; Kukovecz, Á.; Kónya, Z.; Kiricsi, I. *Chem. Mater.* **2007**, *19*, 927–931.
(14) Umek, P.; Korošec, R. C.; Jančar, B.; Dominko, R.; Arčon, D. *J. Nanosci. Nanotechnol.* **2007**, *7*, 3502–3508.
(15) Yuan, Z.-Y.; Su, B.-L. *Colloids Surf. A* **2004**, *241*, 173–183.
(16) Elsanousi, A.; Elssfah, E. M.; Zhang, J.; Lin, J.; Song, H. S.; Tang, C. *J. Phys. Chem. C* **2007**, *111*, 14353–14357.
(17) Ma, R.; Fukuda, K.; Sasaki, T.; Osada, M.; Bando, Y. *J. Phys. Chem. B* **2005**, *109*, 6210–6214.
(18) Ding, Y.; Wang, Z. L. *J. Phys. Chem. C* **2004**, *108*, 12280–12291.
(19) Kukovecz, Á.; Hodos, M.; Kónya, Z.; Kiricsi, I. *Chem. Phys. Lett.* **2005**, *411*, 445–449.
(20) Wei, M.; Konishi, Y.; Zhou, H.; Sugihara, H.; Arakawa, H. *Solid State Commun.* **2005**, *133*, 493–497.

10.1021/cm800077e CCC: $40.75
Published on Web 05/31/2008

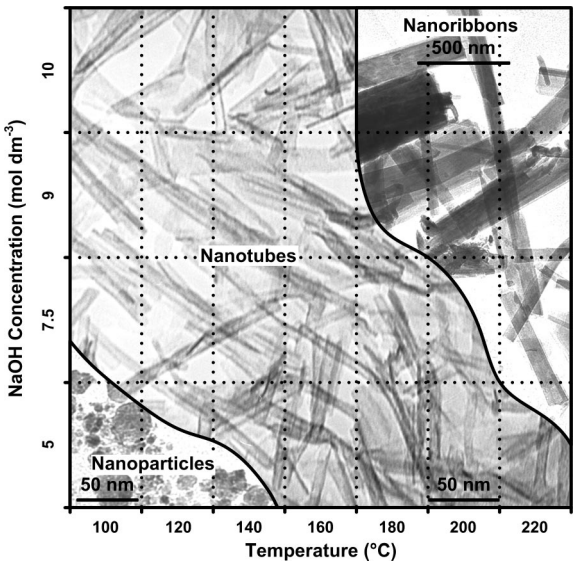

Figure 1. Morphological phase diagram of Degussa P25 indicating regions of nanostructure formation after 20 h of hydrothermal treatment. Phase boundaries were estimated through relative concentrations of nanostructures from XRD and Raman studies, but do not imply contiguous percent morphological phase between each condition.

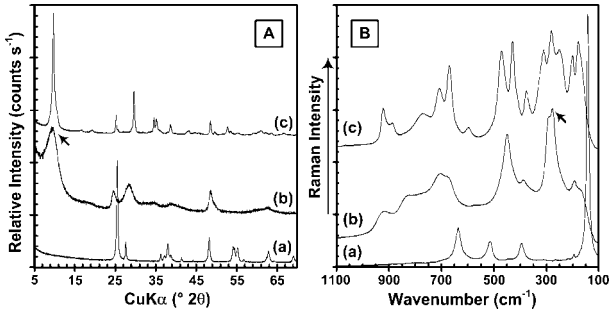

Figure 2. (A) XRD and (B) Raman spectra of (a) Degussa P25, (b) nanotube, and (c) nanoribbon. Arrows indicate peaks relating to nanotube phase.

temperatures and caustic concentrations). Although nanotubes have previously been formed under reduced temperatures,[2b] nanotube formation below 60 °C over 20 h treatment have not been observed.[10a] Degussa P25 was deliberately selected as the titania precursor due to its international availability, and well-characterized physical and chemical properties. As potentials arise for future applications a large industrially sourced precursor is required to produce commercial quantities of titania/titanate nanotubes.

Through the correlation of the X-ray diffraction (XRD) and Raman spectroscopic investigations which were confirmed with transmission electron microscopy (TEM), a morphological phase diagram was determined (Figure 1). Characterization of nanostructure directly through the XRD and Raman was achieved through determining the patterns and spectra typical of nanostructure forms. Figure 2 contains typical patterns of the precursor Degussa P25, synthesized nanotubes and nanoribbons, which have been well-documented.[2a,11,15] To determine the morphological phase diagram, we used the presence of key peaks within the XRD and Raman to detect the presence of different forms of titania/titanate and any alterations in the phase of the nanostructures. Nanotubes were identified through the emergence of the broad, low angle peak between 7.2 and 10.3°

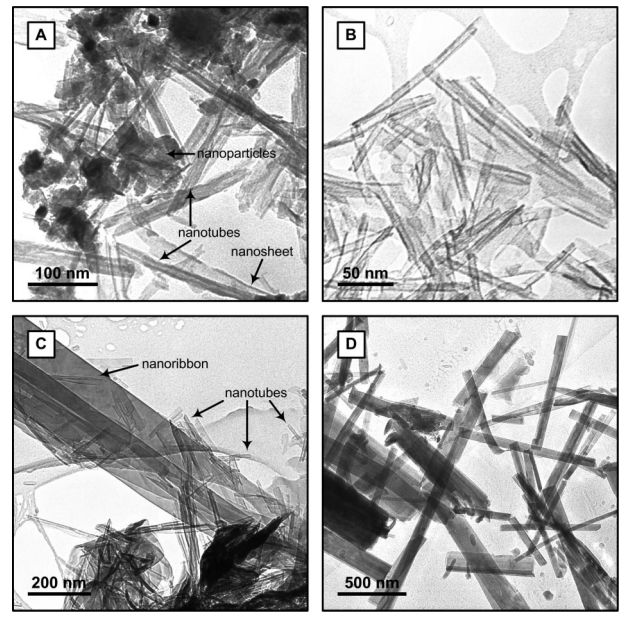

Figure 3. TEM images of (A) nanoparticle/nanotube interface, (B) nanotubes, (C) nanotube/nanoribbon interface, (D) and nanoribbons. Conditions: 5 mol dm^{-3} @ 140 °C, 9 mol dm^{-3} @ 160 °C, 5 mol dm^{-3} @ 220 °C, and 7.5 mol dm^{-3} @ 220 °C, respectively.

2θ in the XRD pattern. This peak may be attributed to the interlayer spacing of the layered titanate phase.[6,21] The Raman spectra of the nanotubes were unique and were dominated by broad, medium intensity peaks. For example, the presence of a peak between 320 and 220 cm^{-1} was considered indicative of nanotube formation even when the spectrum was suffused with anatase. Conversion to nanoribbons was determined in the XRD as an increase in the number and sharpness of reflections that correspond to layered titanates with a monoclinic ($C2/m$) lattice. Depending on the nature of post-treatments, these nanoribbons have previously been assigned to hydrated and nonhydrated analogues of $A_2Ti_nO_{2n+1}$ (where $A = Na^+$ or H^+ and $n = 3$, 4, 5, 9).[10b,11,14–16] An increase in the peak numbers and their relative intensity and sharpness was observed in the nanoribbon spectra in contrast to the nanotube spectra (Figure 2B). These changes were considered to be indicative of the transition from nanotubes to nanoribbons. All three morphological phases contain a consistent layered structure motif, indicating that they comprise related phases.[10b]

The primary morphologies observed within the morphological phase diagram of Figure 1 were nanoparticles, nanotubes, and nanoribbons (Figure 3). Intermediate nanosheet morphology was also observed in conjunction with the nanotubes (Figure 3A), formed through either delamination or dissolution of the titania precursor.[1b,22] These nanosheets scroll or fold into nanotubes once the required driving force has been fulfilled,[3a,22] through the intralayer coordination of undercoordinated Ti and O sites.[23] The phase boundary from

(21) Chen, Q.; Du, G. H.; Zhang, S.; Peng, L.-M. *Acta Crystallogr.* **2002**, *B58*, 587–593.
(22) Wang, Y. Q.; Hu, G. Q.; Duan, X. F.; Sun, H. L.; Xue, Q. K. *Chem. Phys. Lett.* **2002**, *365*, 427–431.
(23) Saponjic, Z. V.; Dimitrijevic, N. M.; Tiede, D. M.; Goshe, A. J.; Zuo, X.; Chen, L. X.; Barnard, A. S.; Zapol, P.; Curtiss, L.; Rajh, T. *Adv. Mater.* **2005**, *17*, 965–971.

nanoparticles to nanotubes was observed to shift to higher temperatures under lower caustic concentrations (5 mol dm^{-3} series, Figure 1). The relative incremental increase of temperature versus concentration suggests that nanotube formation was more dependent on temperature rather than concentration. Past the nanoparticle−nanotube phase boundaries when temperature and caustic concentration were increased, moderate hydrothermal conditions produced high concentrations of nanotubes, with some instances of partially rolled sheets (Figure 3B). These nanotubes had external diameters (8−11 nm, interlayer spacings: 0.76−0.77 nm) and were predominantly scroll-like in nature, with an occasional "onionlike" morphology observed.[3a] Specific variations within a particular structure such as nanotube width with increasing hydrothermal temperature were not observed in this study.[3a,24a]

As the temperature was elevated above 180 °C, a phase transition between nanotubes to nanoribbons was observed. Although nanoribbon formation is believed to be controlled by thermodynamics,[15] analysis of the morphological phase diagram indicated that the effect of temperature was not exclusive in nanoribbon formation: caustic concentration was a significant contributor. This was evident over the caustic concentration range examined with a lower concentration (e.g., 5 and 7.5 mol dm^{-3}) requiring a greater temperature to produce nanoribbons (220 and 200 °C, respectively). Complete conversion to nanoribbons along the phase boundary was observed only in the 10 mol dm^{-3} NaOH sample treated at 180 °C, whereas lower NaOH concentrations exhibited coexistence of both phases (Figure 3C). This indicates that high concentrations of free Na^+ promotes formation of nanoribbons at lower temperatures. Nanoribbons consisted of long plate-like layers with defined edges, high aspect ratios (20−320 nm width, 120−4400 nm length, <5 nm cross-section, and 0.80 nm interlayer spacing) and wide size distributions in each sample (Figure 3D). Most nanoribbons exhibited diffraction contrasts (striations, mottling), suggesting the presence of defects and variations in interlayer spacings caused by interstitial water and ionic species (e.g., Na). Monoclinic structure (*C*2/*m*) was confirmed with a small-area electron diffraction pattern of a single nanoribbon produced in 9 mol dm^{-3} NaOH at 200 °C indexed to $H_2Ti_5O_{11}\cdot 3H_2O$ (JPDF #44−0130) on a $[00\bar{1}]$ zone axis.

Previously, it was implied that at temperatures greater than 150 °C, the pressure may impact on the product formation,[24b] based on calculated NaOH saturation pressures.[25] This study examined hydrothermal temperatures up to 220 °C, which allowed the examination of such pressure effects on nanostructure formation. For NaOH solutions, the vapor pressure of the solution decreases with an increase in the concentration of the analyte. At 100 °C, the saturation pressure of NaOH is 0.8 bar for 5 mol dm^{-3} NaOH and 0.6 bar for 10 mol dm^{-3}. Elevating the temperature to 220 °C the pressure raises to 19.3 and 16.3 bar, respectively.[25] If nanostructure formation was affected by pressure, then lower NaOH concentrations (greater pressure) would promote the formation of nanotubes and nanoribbons. In fact, the opposite trend was observed, indicating that pressure can be excluded as a factor in nanostructure formation.

From inspection of the morphological phase diagram, temperature clearly had the greatest effect on nanostructure formation. Over the temperature range (100−220 °C), both phase boundaries were transected in the 5 and 7.5 mol dm^{-3} series. However, at any given temperature, only one phase boundary was transected when concentration was varied, with the exception of 160 °C, where only nanotubes were produced. Although primarily governed by temperature, the effect of concentration was more subtle in nanotube formation than nanoribbon formation. Between 100 and 140 °C for the 5 mol dm^{-3} NaOH series, latency in nanoparticle consumption and resultant nanotube formation was observed. This suggests that a critical threshold related to concentration must be passed before the nanotubes readily form.

In summary, there is a complex relationship between concentration and temperature affecting formation and that these conditions effect nanotube and nanoribbon formation differently. Understanding this relationship will further elucidate the mechanism of titanate nanostructure formation. The morphological phase diagram in this study is a useful guide for synthesizing one-dimensional titanate nanostructures and controlling the product morphology.

Supporting Information Available: Full Raman spectra and XRD patterns for the determinaion of the morphological phase diagram (PDF). This information is avaliable free of charge via the Internet at http://pubs.acs.org.

CM800077E

(24) (a) Tsai, C.-C.; Teng, H. *Chem. Mater.* **2004**, *16*, 4352–4358. (b) Tsai, C.-C.; Teng, H. *Chem. Mater.* **2006**, *18*, 367–373.

(25) Perry, R. H. ; Green, D. W. ; Maloney, J. O. , *Perry's Chemical Engineers' Handbook*, 7th ed.; McGraw-Hill: New York, 1997.